Multi-area Frequency-constrained Unit Commitment for Power Systems with High Penetration of Renewable Energy Sources and Induction Machine Load

Leibao Wang, Hui Fan, Jifeng Liang, Longxun Xu, Tiecheng Li, Peng Luo, Bo Hu, and Kaigui Xie

***Abstract*—The increasing penetration of renewable energy sources (RESs) brings great challenges to the frequency security of power systems. The traditional frequency-constrained unit commitment (FCUC) analyzes frequency by simplifying the average system frequency and ignoring numerous induction machines (IMs) in load, which may underestimate the risk and increase the operational cost. In this paper, we consider a multi-area frequency response (MAFR) model to capture the frequency dynamics in the unit scheduling problem, in which regional frequency security and the inertia of IM load are modeled with high-dimension differential algebraic equations. A multi-area FCUC (MFCUC) is formulated as mixed-integer nonlinear programming (MINLP) on the basis of the MAFR model. Then, we develop a multi-direction decomposition algorithm to solve the MFCUC efficiently. The original MINLP is decomposed into a master problem and subproblems. The subproblems check the nonlinear frequency dynamics and generate linear optimization cuts for the master problem to improve the frequency security in its optimal solution. Case studies on the modified IEEE 39-bus system and IEEE 118-bus system show a great reduction in operational costs. Moreover, simulation results verify the ability of the proposed MAFR model to reflect regional frequency security and the available inertia of IMs in unit scheduling.**

***Index Terms*—Decomposition algorithm, frequency response, frequency-constrained unit commitment, induction machine, multi-area, mixed-integer nonlinear programming (MINLP).**

NOMENCLATURE

A. Indices and Sets

*	Per-unit values
Ω_j	Set of bus indices for area j
Δ	Index of variations, deviations, and increments
$\tau 0$, τ	Indices of initial values and current values
A	Set of tie-lines
i	Index of generators
j, k	Indices of areas
n	Index of iterations
t	Index of time intervals
$\hat{x}$	Value of variables x in the solution to current master problem

B. Parameters

μ_{G}^{-1}	Unit regulating power of synchronous generators (SGs)
λ	Ratio of induction machine (IM) load to the total load in area j (default value as 0.6)
$a_i^{\mathrm{G}}, b_i^{\mathrm{G}}$	Fuel cost factors of SG unit i
$c_i^{\mathrm{G}}, d_i^{\mathrm{G}}$	Up and down reserve factors of SG unit i
$C_{\mathrm{W}}, C_{\mathrm{PV}}$	Penalty factors of wind and photovoltaic (PV) curtailment
F_{HP}	Fraction of total power generated by the turbine of SGs
$f_{\infty,\min}$	Security threshold of settling frequency index
f_{base}	Rated frequency of power systems
$f_{\mathrm{nadir,min}}$	Security threshold of frequency nadir index
H_{im}	Rotor inertia of IMs
H_{sg}	Rotor inertia of SGs
Ke	Load rate of IMs
k_L	Load regulating factor
N_{G}	Number of SG units
$N_{\mathrm{W}}, N_{\mathrm{PV}}$	Number of wind plants and PV stations
$P_{N,i}^{\mathrm{G}}$	Rated capacity of SG unit i
P_N^{IM}	Rated capacity of IMs
$RoCoF_{\max}$	Security threshold of rate of change of frequency (RoCoF) index

Manuscript received: January 3, 2023; revised: May 14, 2023; accepted: June 27, 2023. Date of CrossCheck: July 23, 2023. Date of online publication: August 29, 2023.

This work was supported by the Science and Technology Project of State Grid Hebei Electric Power Company Limited (No. kj2021-073).

L. Wang (corresponding author), H. Fan, J. Liang, T. Li, and P. Luo are with the State Grid Hebei Electric Power Research Institute, Shijiazhuang 050021, China (e-mail: leibaowang1993@163.com; fanh@he.sgcc.com.cn; ljifeng@126.com; ltc8086@163.com; luopeng1984@sohu.com).

L. Xu, B. Hu, and K. Xie are with State Key Laboratory of Power Transmission Equipment and System Security, Chongqing University, Chongqing 400044, China (e-mail: xulx@cqu.edu.cn; hboy8361@163.com; kaiguixie@vip.163.com).

DOI: 10.35833/MPCE.2023.000002

S_i^{G} Startup cost of SG unit i

T Number of periods in multi-area frequency-constrained unit commitment (MFCUC)

T_1, T_2, K Parameters in inertia of IM model

$T_{j\text{-}k}$ Ratio of variation of transmission power to phase angle difference between areas j and k

T_R Reheat time constant of SGs

X_{l_1} Impedance of line l_1

C. Variables

$\Delta\theta$ Increment of bus phase angle

ΔF_{l_1} Variation of power flow on line l_1

ΔP_{Dj} Power deviation in area j

ΔP_E Deviation of electromagnetic power in primary frequency response (PFR)

ΔP_L^* Deviation of load on actual frequency

ΔP_{LN}^* Deviation of load on rated frequency

ΔP_{RES} Fluctuation of renewable energy source (RES) generation

ΔP_{Tj} Total power that is transmitted from area j to neighboring areas

ω_r^* Rotation speed of IMs

ω_s^* Synchronous speed of SGs

$C_{\infty,\tau}$ Total sensitivity of f_∞ index at time τ

$C_{\mathrm{G,run}}$ Operation cost in objective function

$C_{\mathrm{G,re}}$ Reserve cost in objective function

$C_{\mathrm{G,start}}$ Startup cost of SGs in objective function

$C_{\mathrm{nadir},\tau}$ Total sensitivity of f_{nadir} index at time τ

C_{RES} RES curtailment cost in objective function

$C_{\mathrm{RoCoF},\tau}$ Total sensitivity of RoCoF index at time τ

FI_τ Frequency index at time τ

f^* System frequency

f_∞ Settling frequency

f_{nadir} Frequency nadir

$H_{\Sigma,\tau}, K_{\Sigma,\tau}$ Total inertia and unit regulating power at time τ

M_{im} Available inertia of IMs

P_{sgM}^* Mechanical power of SGs

P_{sgE}^* Electromagnetic power of SGs

P_{imM}^* Mechanical power of IMs

P_{imE}^* Electromagnetic power of IMs

$P_{i,\tau}^{\mathrm{G}}$ Generation of SG unit i at time τ

$P_{i,\tau}^{\mathrm{G,up}}, P_{i,\tau}^{\mathrm{G,down}}$ Up and down reserves of SG unit i at time τ

$P_{LN,k\tau}$ Load of bus k on rated frequency at time τ

$P_{i,\tau}^{\mathrm{W,f}}, P_{i,\tau}^{\mathrm{PV,f}}$ Forecast generation of wind and PV

$P_{i,\tau}^{\mathrm{W}}, P_{i,\tau}^{\mathrm{PV}}$ Real generation of wind and PV

$RoCoF$ Value of RoCoF index

$S_{\infty,i\tau}$ Sensitivity of f_∞ index to status of SG unit i at time τ

$S_{\mathrm{FI},i\tau}$ Sensitivity of frequency indices to status of SG unit i at time τ

$S_{\mathrm{nadir},i\tau}$ Sensitivity of f_{nadir} index to status of SG unit i at time τ

$S_{\mathrm{RoCoF},i\tau}$ Sensitivity of RoCoF index to status of SG unit i at time τ

$u_{i,\tau}^{\mathrm{G}}$ Binary variable of commitment status of SG unit i at time τ (equals 1 if unit is on and 0 otherwise)

$\boldsymbol{u}_\tau^{\mathrm{G}}$ Vector of commitment status of SG units at time τ

I. Introduction

With the aggravation of the global climate issue, low-carbon development has become the consensus of most countries. In 2020, China put forward the goals of carbon peak and carbon neutrality to address this global problem. In this context, the penetration of renewable energy sources (RESs) is gradually increasing while the utilization of fossil and coal resources is being reduced in power systems. While the increasing penetration of RESs reduces greenhouse gas emissions and fuel costs, it also brings new challenges to the security of power systems. Compared with traditional synchronous generators (SGs), RES generators provide weak inertia and lack the ability for PFR. Moreover, the uncertainties of RES worsen the power balance problems. Therefore, it is difficult for power systems with a high penetration of RES to tolerate a large frequency deviation [1]. For instance, both the South Australia blackout on September 28, 2016 [2] and the British blackout on August 9, 2019 [3] were induced by frequency issues. As a result of the blackouts, the former lost a load of 1826 MW for 50 hours, while the latter curtailed a load of nearly 1000 MW. As the unit commitment (UC) for 24 hours determines the pre-contingency operating status of power systems and also dominates the system frequency response (SFR) for several seconds during the contingency, it is essential to consider the frequency security constraints in UC.

At present, most studies on frequency-constrained unit commitment (FCUC) analyze frequency dynamics according to the center of inertia (COI) principle. After ignoring the spatial distribution characteristic of power system frequency, the COI principle usually assumes that the frequency in the whole system is unique and is regarded as the average frequency of the system [4]. Based on COI, frequency response models such as the average system frequency (ASF) model [5] and its simplification and the SFR model [6] are successively proposed. The governor and prime mover models of generators are aggregated in the PFR of generators into the SFR model, and the mechanical dynamics of the multi-machine system are simplified to those of a single-machine system. This can simplify the frequency model of power systems so that the analytical constraints of frequency security can be constructed. However, the COI principle that the entire system shares a frequency may lead to significant errors in large systems with an uneven inertia distribution [7]. With the ASF model or the SFR model, three frequency security

indices can be analyzed in the constraints of FCUC, namely, the rate of change of frequency (RoCoF), the frequency nadir f_{nadir}, and the settling frequency f_{∞} [8].

Considering the highly nonlinear calculations of frequency security indices of power systems, the FCUC is mostly modeled with mixed-integer nonlinear programming (MINLP), which cannot be solved efficiently by commercial solvers. In [9] and [10], the complicated frequency index constraints are substituted with constraints, such as inertia, kinetic energy, and available synchronous capacity. These constraints can be represented in a simple form. However, as the frequency security is measured indirectly, it is difficult for the results of FCUC to guarantee accuracy. In addition, intelligent algorithms such as particle swarm optimization [11], deep neural network [12], optimal classification trees [13], and genetic algorithm [14] are also used to solve the nonlinear FCUC model. Although these algorithms can solve the MINLP model directly, they may get stuck in local optimum solutions.

Many linearization techniques are also adopted to handle the constraints of frequency security indices, with which the FCUC can be converted to mixed-integer linear programming (MILP). Separable programming is used in [15] to linearize the frequency index f_{nadir} by translating it into a larger linear program that involves additional binary variables. The data-driven piecewise linearization method is adopted in [16] to handle the highly nonlinear frequency constraints with a mixed-integer second-order cone problem of hyperplane fitting and data classification. Similarly, [17] and [18] use piecewise linearization to linearize the frequency function by introducing an MILP problem. In [19], an assumption that f_{nadir} is a linear function of RoCoF is utilized, with which f_{nadir} can be linearized. Although these linearization techniques can develop the MILP that is easier to solve, they are limited to the simplified system frequency model and cannot deal with complicated multi-area frequency dynamics.

Recently, the decomposition optimization framework has also been introduced to the FCUC [20]. The original MINLP model is decomposed into a master problem and several subproblems. The master problem solves UC with optimization cuts from the subproblems as a substitution of the nonlinear frequency constraints. The subproblems update the optimization cuts of frequency indices for the current solution to the master problem. The master problem and subproblems are solved iteratively until the optimal solution is found. In [21], the two-stage stochastic FCUC is decomposed with the L-shape algorithm, in which the subproblems check the frequency security and generate the feasibility cuts and optimality cuts for the master problem. In [22], an improved tri-level Benders decomposition algorithm is proposed to optimize the primary and secondary frequency responses. Reference [23] uses the cuts of unit regulating power to represent the frequency response ability of systems. The practicality of these methods for FCUC with the COI principle has been verified. However, the decomposition optimization framework for multi-area FCUC (MFCUC) remains to be developed.

Although the above studies provide powerful tools for FCUC, there are some limitations. Firstly, frequency analysis with COI may induce an underestimate of frequency security risk as it ignores the difference in frequency responses in different areas, especially for large-scale systems. Secondly, the load of power systems has complicated frequency response properties. In existing FCUC models, the load is usually aggregated, and only its PFR is modeled as a proportional element. However, studies have shown that the induction machines (IMs) in load can also provide inertia support during disturbances [24], [25]. As the IMs account for a large proportion (usually 50%-70%) of the load, the FCUC needs to incorporate the inertial response of IMs into frequency dynamics analysis. It is especially valuable in receiving-end power systems with a high penetration of renewables. This is because the number of SGs in the receiving-end power systems is significantly less than that in the sending-end power systems. In addition, the integration of renewable energy further reduces the inertia from SGs in receiving-end power systems.

In this context, this paper proposes an MFCUC model considering the inertia of IMs. The main contributions are summarized as follows:

1) The frequency dynamics of IMs is modeled in the FCUC by incorporating the inertia support of IMs into the system inertia response. The RoCoF and frequency nadir are improved by the available inertia of IMs, and thus the operational cost for frequency security enhancement is also reduced. It improves the tolerability of power systems for large frequency disturbances, especially those lacking inertia from SGs.

2) The multi-area frequency response (MAFR) model is considered to develop the MFCUC considering the inertia of IMs. Compared with the COI-based SFR model, the differences in frequency dynamics between areas are accurately modeled in the proposed model.

3) A multi-direction decomposition algorithm for solving the MFCUC efficiently is proposed. In addition to traditional optimization cuts, sensitivity cuts are proposed to further enhance the robustness of the decomposition algorithm for MFCUC.

The structure of this paper is organized as follows. Section II introduces the frequency response model. Section III proposes the MFCUC model, and Section IV discusses the solution to MFCUC model. Finally, case studies are performed in Section V and conclusions are drawn in Section VI.

II. Frequency Response Model

A. Frequency Response Model for SGs and Load

In security assessment studies, the frequency dynamics of power systems is dominated by the response of generators and loads. It should be noted firstly that only conventional SG units and loads participate in frequency response in this paper, while RES generators are not considered as assumed in most studies.

The SGs exchange power with the grid through the change of amplitude and phase of electromotive force (EMF). According to the physical mechanism of SGs, the

stator and rotor flux rotate at a synchronous speed, which makes the phase of EMF and the rotor position relatively static. After ignoring the damping factor of SGs, the phase motion of EMF can be directly expressed by the rotor motion equation (1).

$$2H_{sg}\frac{\mathrm{d}\omega_s^*}{\mathrm{d}t}=P_{sgM}^*-P_{sgE}^* \tag{1}$$

In the per-unit form, the system frequency f^* is equal to ω_s^*. Therefore, the frequency response model in the complex frequency domain is:

$$2H_{sg}s\Delta f^*=\Delta P_{sgM}^*-\Delta P_{sgE}^* \tag{2}$$

The mechanical power deviation ΔP_{sgM}^* of SGs in the lower-order generator model [6] is calculated as:

$$\Delta P_{sgM}^*=-\frac{1}{\mu_{\mathrm{G}}}\frac{1+sF_{HP}T_R}{1+sT_R}\Delta f^* \tag{3}$$

In most studies on frequency security, the inertia of load is ignored, and it is only modeled in the PFR as:

$$\Delta P_L^*=\Delta P_{LN}^*+k_L\Delta f^* \tag{4}$$

B. Inertial Response Model of IMs

It is noted that the frequency response model of load only includes the PFR, and its inertia response is neglected. For power systems with high penetration of RESs, the total inertia from SGs decreases with the increase of electric power generation from RES. Although the inertia of loads is smaller compared with that of SGs, it is of great significance for frequency security. In power systems, IMs account for a large proportion that is not less than 50% of the load. It has been found that IMs are able to provide inertial support like SGs when power deviation occurs [24], [25]. The modeling of the inertia of IMs can help improve the frequency security indices in FCUC and thus may further reduce the operational cost. In this subsection, the inertial response model of IMs is introduced and will be incorporated into the following MAFR model.

Firstly, the rotor motion equation of IMs is expressed as (5), which is the same as that of SGs.

$$2H_{im}\frac{\mathrm{d}\omega_r^*}{\mathrm{d}t}=P_{imM}^*-P_{imE}^* \tag{5}$$

In IMs, the phase of the EMF and the position of the rotor are asynchronous owing to the slip between the stators and the rotors. The rotor motion equation (5) in IMs cannot describe the phase motion of EMF and the active power. To describe the phase motion of EMF like SGs, the available inertia of IMs is proposed in [24], [25] for frequency response analysis of power systems. By this way, the phase motion equation of EMF in the complex frequency domain is:

$$M_{im}s\Delta f^*=\Delta P_{imM}^*-\Delta P_{imE}^* \tag{6}$$

The available inertia of IMs in (6) is defined as:

$$M_{im}(s)=2H_{im}G(s) \tag{7}$$

$$G(s)=\frac{s+T_2}{T_1s+1}\frac{K}{s} \tag{8}$$

It can be found from (8) that the available inertia of IMs is affected by both rotor inertia and slip frequency regulation. In contrast to the inertia of SGs, which is constant in frequency response analysis, the available inertia of IMs has a time-varying property. More details can be found in [24], [25].

C. COI-based SFR Model with IMs

The COI-based SFR model is widely adopted in the frequency security assessment of power systems, which is shown in Fig. 1. To integrate the frequency response constraints into UC, a power disturbance is set in the power system on each hour, and then the frequency security is checked [20]. The amount of power disturbance on each hour can be set according to forecast errors of load and renewable energy [17], generator outages [12], voltage source converter based multi-terminal direct current outage [26]. In this paper, we consider the power deviation induced by the load fluctuation ΔP_L and the RES fluctuation ΔP_{RES} for frequency security assessment. If we ignore the transmission loss, the total power deviation is also equal to the deviation of electromagnetic power ΔP_E in PFR.

$$\Delta P_E=\Delta P_L+\Delta P_{RES}=\sum_{i=1}^{N_{\mathrm{G}}}\Delta P_{sgE,i}+\Delta P_{imE} \tag{9}$$

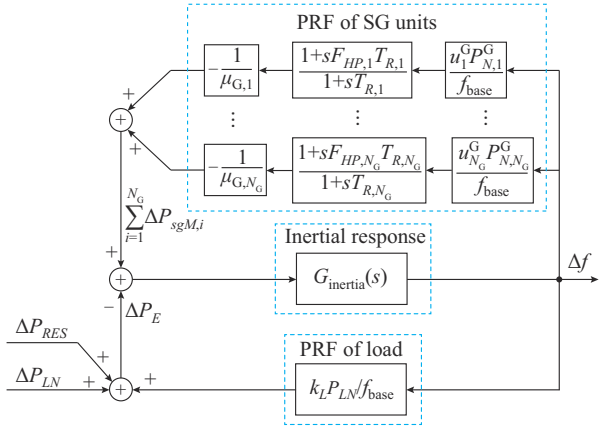

Fig. 1. COI-based SFR model with IMs.

In this paper, the massive IM units in power systems with different rated voltage levels are aggregated in the analysis of inertia response. Considering the available inertia of IMs in (7), the transfer function of inertial response $G_{\mathrm{inertia}}(s)$ in Fig. 1 can be expressed as:

$$G_{\mathrm{inertia}}(s)=\frac{f_{\mathrm{base}}}{2\sum_{i=1}^{N_{\mathrm{G}}}u_i^{\mathrm{G}}P_{N,i}^{\mathrm{G}}H_{sg,i}s+P_N^{\mathrm{IM}}M_{im}s} \tag{10}$$

D. MAFR with IMs

It has been demonstrated in [7] that the post-contingency frequency dynamics of a multi-area grid consists of two parts, namely, the frequency evolution of the COI and certain inter-area oscillations. Certain inter-area oscillations are caused by the uneven distribution of generator inertia in different areas [7]. As the COI-based SFR model can only capture the average frequency dynamics in multi-area power systems with uneven inertia distribution, it may lead to conservative UC schemes in the areas with high inertia and the vio-

lation risk of frequency security in the areas with low inertia. It is more practical to construct an MAFR model with IMs.

Unlike the COI-based SFR model, the MAFR model divides a system into several areas, and then each area is represented by its average frequency. Figure 2 shows the frequency response in area j of MAFR model with IMs.

$$\Delta P_{Dj} = \Delta P_{RESj} + \Delta P_{LNj} \tag{11}$$

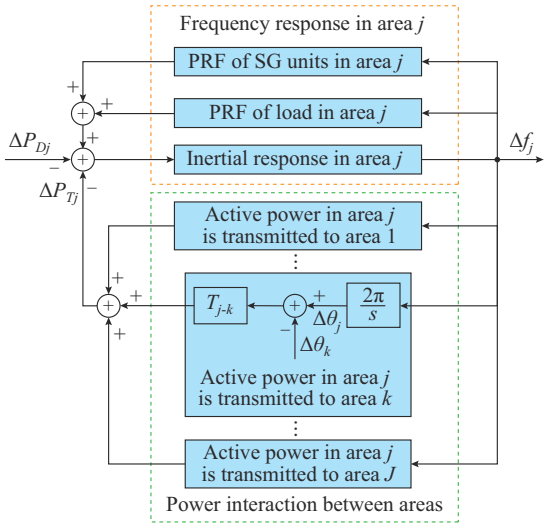

Fig. 2. Frequency response in area j of MAFR model with IMs.

As shown in Fig. 2, the frequency response in area j includes two parts. The first part is the frequency response in area j, which can be modeled as the COI-based SFR model. Namely, all buses in area j have the same variation of voltage phase angle. The second part is the power interactions between area j and other areas. Suppose that there is a tie line l_1 between the areas j and k. The transmission power between areas j and k can be calculated as (12) if we simplify the AC power flow in [27] by DC power flow.

$$\Delta F_{l_1} = \frac{\Delta\theta_a - \Delta\theta_b}{X_{l_1}} = \frac{2\pi\int\left(\Delta f_j - \Delta f_k\right)\mathrm{d}t}{X_{l_1}} \tag{12}$$

where buses a and b are in areas j and k, respectively.

In the complex frequency domain, we have the Laplace transform of (12) as (13).

$$\Delta F_{l_1}(s) = \frac{2\pi T_{j\text{-}k}}{s}\left(\Delta f_j - \Delta f_k\right) \tag{13}$$

$$T_{j\text{-}k} = \frac{1}{X_{l_1}} \tag{14}$$

If there are multiple tie-lines between areas j and k, it is easy to have the parameter $T_{j\text{-}k}$ as (15).

$$T_{j\text{-}k} = \sum_{l\in A}\frac{1}{X_l} \tag{15}$$

The frequency response in area j of MAFR model with IMs in Fig. 2 is constructed to simulate the frequency security constraints in MFCUC in Section III-B.

III. MFCUC Model

The MFCUC model considering the inertia of IMs is proposed with the MAFR. The objective function of the proposed MFCUC model is to minimize the operational cost under the operational constraints of power systems and area frequency security constraints.

A. Objective Function

The objective function of the MFCUC model is constructed as (16)-(20).

$$\min F = C_{\mathrm{G,run}} + C_{\mathrm{G,re}} + C_{\mathrm{G,start}} + C_{RES} \tag{16}$$

$$C_{\mathrm{G,run}} = \sum_{\tau=1}^{T}\sum_{i=1}^{N_{\mathrm{G}}}\left(a_i^{\mathrm{G}}P_{i,\tau}^{\mathrm{G}} + b_i^{\mathrm{G}}u_{i,\tau}^{\mathrm{G}}\right) \tag{17}$$

$$C_{\mathrm{G,re}} = \sum_{\tau=1}^{T}\sum_{i=1}^{N_{\mathrm{G}}}\left(c_i^{\mathrm{G}}P_{i,\tau}^{\mathrm{G,up}} + d_i^{\mathrm{G}}P_{i,\tau}^{\mathrm{G,down}}\right) \tag{18}$$

$$C_{\mathrm{G,start}} = \sum_{\tau=1}^{T-1}\sum_{i=1}^{N_{\mathrm{G}}}\frac{S_i^{\mathrm{G}}}{2}\left[\left(u_{i,\tau+1}^{\mathrm{G}} - u_{i,\tau}^{\mathrm{G}}\right) + \left|u_{i,\tau+1}^{\mathrm{G}} - u_{i,\tau}^{\mathrm{G}}\right|\right] \tag{19}$$

$$C_{RES} = \sum_{\tau=1}^{T}\left[C_{\mathrm{W}}\sum_{i=1}^{N_{\mathrm{W}}}\left(P_{i,\tau}^{\mathrm{W,f}} - P_{i,\tau}^{\mathrm{W}}\right) + C_{\mathrm{PV}}\sum_{i=1}^{N_{\mathrm{PV}}}\left(P_{i,\tau}^{\mathrm{PV,f}} - P_{i,\tau}^{\mathrm{PV}}\right)\right] \tag{20}$$

B. Constraints

The operational constraints of SGs include the generation limits, the up and down reserve limits, the ramp rate limits, and the minimum startup and shutdown time limits. The first three constraints can be found in [28], while the minimum startup and shutdown time limits can be found in [29]. In addition, considering the uncertainty of load and RES, the total reserve in power systems is also required to be larger than the sum of the forecast errors. The constraint of total system reserve capacity can be set with a reserve factor, as in [28]. The generation constraints of wind plants and PV stations can be found in [30]. In this paper, we consider the case that the actual generation of renewable energy is limited by the forecasted value. To make the system operate in the scheduled security region, the power system operators choose to curtail some renewable generation when it is higher than the forecasted value. Network constraints, including transmission capacity limits, phase angle limits, and active power balance, can be found in [28].

Compared with the low-frequency issue, the over-frequency issue can be mitigated more practically by tripping the renewable plants or the SGs to eliminate the excessive power in the power system. The low-frequency issue is more challenging in power systems with high penetration of renewable energy due to the lack of inertia from renewable energy. Thus, in this paper, the frequency security constraints for area j are described with the limits of three low-frequency indices, which are expressed as:

$$RoCoF_{j,\tau} \le RoCoF_{\max} \tag{21}$$

$$f_{\mathrm{nadir},j,\tau} \ge f_{\mathrm{nadir,min}} \tag{22}$$

$$f_{\infty,j,\tau} \ge f_{\infty,\min} \tag{23}$$

In this paper, the frequency dynamics is simulated with the Simulink toolbox in MATLAB. As shown in Fig. 2, the startup and shutdown status of generating units in each area is required by the simulation of the MAFR model. Mean-

while, the violations of constraints (21)-(23) also make the MFCUC model adjust the generator status in each area. When the simulation is completed, the frequency indices in constraints (21)-(23) can be directly calculated from the system frequency dynamic record. The value of RoCoF is calculated with 10 subsequent cycles, i.e., 200 ms at 50 Hz [31]. The value of the frequency nadir is identified as the maximum frequency deviation in the record. The value of the settling frequency is identified as the frequency deviation at the end of the simulation.

IV. Solution to MFCUC Model

As the available inertia of IMs in (7) is highly nonlinear in the time domain, it is difficult to derive the analytical formula of three frequency indices in (21)-(23). This makes it rather challenging to efficiently solve the MFCUC with the inertia of IMs. Thus, a decomposition algorithm is constructed in this section. Firstly, we review the classical decomposition algorithm in existing studies on solving the FCUC with the COI principle. Then, to address the multiple-area frequency issues, we propose a new optimization cut based on sensitivity analysis in the decomposition algorithm. Finally, a multi-direction optimization framework using parallel calculation is proposed to improve the robustness of MFCUC solutions.

A. Decomposition Algorithms for FCUC with COI Principle

Since constraints (21)-(23) are nonlinear and not analytical, it is difficult for commercial optimization solvers to solve the FCUC model directly. As the decomposition algorithms are powerful tools to solve the MINLP, they have been developed for solving the FCUC with the COI principle [20]. Generally, the original FCUC model is decomposed into a master problem and several subproblems. The master problem is the FCUC without consideration of constraints (21)-(23), which is linear and can be efficiently solved. The solution to the master problem determines the SFR capability. The subproblem is constructed to check whether constraints (21)-(23) are satisfied for the solution to the current master problem. If the current solution to the master problem fails to satisfy constraints (21)-(23), an optimization cut is generated and added to the master problem to improve the frequency security of its solution. The decomposition algorithm is terminated when constraints (21)-(23) are satisfied or no feasible solution can be found.

In the decomposition algorithms for FCUC, the inertia H_{sg} and the unit regulating power μ_{G}^{-1} are widely used to quantify the frequency response ability. Correspondingly, when constraints (21)-(23) are not satisfied at time τ, the optimization cuts can be generated as [23]:

$$H_{\Sigma,\tau} > \hat{H}_{\Sigma,\tau} \tag{24}$$

$$K_{\Sigma,\tau} > \hat{K}_{\Sigma,\tau} \tag{25}$$

Here, $H_{\Sigma,\tau}$ and $K_{\Sigma,\tau}$ are defined as:

$$H_{\Sigma,\tau} = \sum_{i=1}^{N_{\mathrm{G}}} u_{i,\tau}^{\mathrm{G}} H_{sg,i} \tag{26}$$

$$K_{\Sigma,\tau} = \sum_{i=1}^{N_{\mathrm{G}}} u_{i,\tau}^{\mathrm{G}} \mu_{\mathrm{G},i}^{-1} \tag{27}$$

B. Multi-direction Optimization Framework with Sensitivity Cuts for MFCUC

As the sensitivity cuts of inertia and unit regulating power only assess frequency security indirectly and are mainly designed for the FCUC with the COI principle, the optimization cuts (24) and (25) may lead to suboptimal solutions when the MAFR is considered. In this context, we propose a series of cuts based on the sensitivities of system frequency indices to further improve the robustness of the decomposition algorithm for MFCUC.

Firstly, let function g denote the MAFR model in Section II-D, which is given as:

$$FI_{\tau} = g\left(\boldsymbol{u}_{\tau}^{\mathrm{G}}\right) \tag{28}$$

In this paper, the sensitivity of frequency indices to the commitment status of unit i at time τ, $S_{\mathrm{FI},i\tau}$, is defined as the first-order analytic derivative of function g at the MFCUC solution $\boldsymbol{u}_{\tau}^{\mathrm{G}}$. With the sensitivity definition, (28) can be approximated as (29).

$$FI_{\tau 0} \approx g\left(\boldsymbol{u}_{\tau 0}^{\mathrm{G}}\right) + \sum_{i=1}^{N_{\mathrm{G}}} S_{\mathrm{FI},i\tau} \Delta u_{i,\tau}^{\mathrm{G}} \tag{29}$$

As function g is highly nonlinear and includes binary variables, it is rather difficult to accurately get its first-order analytic derivative. Thus, a simulation-based numerical analysis method is used to calculate the sensitivity in this paper. The steps are described as follows.

Firstly, when the frequency security constraints are violated at time τ, we approximate the sensitivities of frequency indices to the commitment status of SG units as (30)-(32).

$$S_{\mathrm{RoCoF},i\tau} = \frac{RoCoF_{i\tau} - RoCoF_{\tau 0}}{u_{i,\tau}^{\mathrm{G}} - u_{i,\tau 0}^{\mathrm{G}}} \tag{30}$$

$$S_{\mathrm{nadir},i\tau} = \frac{f_{\mathrm{nadir},i\tau} - f_{\mathrm{nadir},\tau 0}}{u_{i,\tau}^{\mathrm{G}} - u_{i,\tau 0}^{\mathrm{G}}} \tag{31}$$

$$S_{\infty,i\tau} = \frac{f_{\infty,i\tau} - f_{\infty,\tau 0}}{u_{i,\tau}^{\mathrm{G}} - u_{i,\tau 0}^{\mathrm{G}}} \tag{32}$$

Then, we use the numerical simulation to acquire the index value $RoCoF_{i\tau}$ following the change of commitment status of unit i. In the numerical simulation, the principle for setting the change of commitment status of unit i is described as follows.

1) If $u_{i,\tau 0}^{\mathrm{G}} = 0$, we have $u_{i,\tau}^{\mathrm{G}} = 1$. Namely, when the SG unit i is not committed in $\boldsymbol{u}_{\tau 0}^{\mathrm{G}}$, its status is changed to be committed in $\boldsymbol{u}_{\tau}^{\mathrm{G}}$.

2) If $u_{i,\tau 0}^{\mathrm{G}} = 1$, we have $u_{i,\tau}^{\mathrm{G}} = 0$. Namely, when the SG unit i is committed in $\boldsymbol{u}_{\tau 0}^{\mathrm{G}}$, its status is changed to be not committed in $\boldsymbol{u}_{\tau}^{\mathrm{G}}$.

After simulating the frequency response with the updated commitment status of the unit i, the sensitivities of frequency indices can be calculated as (30)-(32).

Compared with the amount of inertia and unit regulating capacity, the sensitivities provide more direct optimization in-

formation for frequency security improvement. Thus, the optimization cuts based on the sensitivities are proposed as follows.

Suppose $\boldsymbol{u}_{\tau}^{\mathrm{G}}(n)$ is the solution to the master problem in the n^{th} iteration. The solution in the next iteration can be denoted as:

$$\boldsymbol{u}_{\tau}^{\mathrm{G}}(n+1)=\boldsymbol{u}_{\tau}^{\mathrm{G}}(n)+\Delta\boldsymbol{u}_{\tau}^{\mathrm{G}} \tag{33}$$

As the frequency indices in the $(n+1)^{\mathrm{th}}$ iteration should be improved, we have the following constraints:

$$RoCoF_{\tau}(n+1)<RoCoF_{\tau}(n) \tag{34}$$

$$f_{\mathrm{nadir},\tau}(n+1)>f_{\mathrm{nadir},\tau}(n) \tag{35}$$

$$f_{\infty,\tau}(n+1)>f_{\infty,\tau}(n) \tag{36}$$

Considering (29)-(32), we can obtain:

$$\sum_{i=1}^{N_{\mathrm{G}}}S_{\mathrm{RoCoF},i\tau}\Delta u_{i,\tau}^{\mathrm{G}}<0 \tag{37}$$

$$\sum_{i=1}^{N_{\mathrm{G}}}S_{\mathrm{nadir},i\tau}\Delta u_{i,\tau}^{\mathrm{G}}>0 \tag{38}$$

$$\sum_{i=1}^{N_{\mathrm{G}}}S_{\infty,i\tau}\Delta u_{i,\tau}^{\mathrm{G}}>0 \tag{39}$$

Finally, the optimization cuts are derived as:

$$C_{\mathrm{RoCoF},\tau}<\hat{C}_{\mathrm{RoCoF},\tau} \tag{40}$$

$$C_{\mathrm{nadir},\tau}>\hat{C}_{\mathrm{nadir},\tau} \tag{41}$$

$$C_{\infty,\tau}>\hat{C}_{\infty,\tau} \tag{42}$$

$$C_{\mathrm{RoCoF},\tau}=\sum_{i=1}^{N_{\mathrm{G}}}S_{\mathrm{RoCoF},i\tau}u_{i,\tau}^{\mathrm{G}} \tag{43}$$

$$C_{\mathrm{nadir},\tau}=\sum_{i=1}^{N_{\mathrm{G}}}S_{\mathrm{nadir},i\tau}u_{i,\tau}^{\mathrm{G}} \tag{44}$$

$$C_{\infty,\tau}=\sum_{i=1}^{N_{\mathrm{G}}}S_{\infty,i\tau}u_{i,\tau}^{\mathrm{G}} \tag{45}$$

Figure 3 shows the calculation flowchart of the proposed sensitivity cuts for MFCUC. Firstly, the master problem is solved to provide an initial UC scheme. Then, with the generator status from the solution to master problem, the subproblem uses the Simulink toolbox to acquire the frequency dynamic record following the power disturbance each hour. The frequency indices in constraints (21)-(23) are directly checked with the system frequency dynamic record. When constraints (21)-(23) are violated, the proposed sensitivity cuts are generated. It should be noted that when there are multiple violations of frequency security, we generate the sensitivity cuts (40)-(42) for the area with the worst violation. Once more, the master problem is solved again after the optimization cuts is updated. The loop in Fig. 3 is performed until the solution to master problem does not violate the constraints (21)-(23) during all periods.

With the construction of the sensitivity cuts for MFCUC, the proposed multi-direction method in Fig. 4 is adopted to further improve the robustness of the decomposition algorithms. When the frequency security constraints are not satisfied, the optimal solution to MFCUC is searched in three directions. In each direction, an MILP problem is generated by adding the inertia cut (24), unit regulating power cut (25) or the proposed sensitivity cuts (40)-(42). After all MILP problems in three directions are solved in parallel, the most economical scheme is selected as the optimal solution.

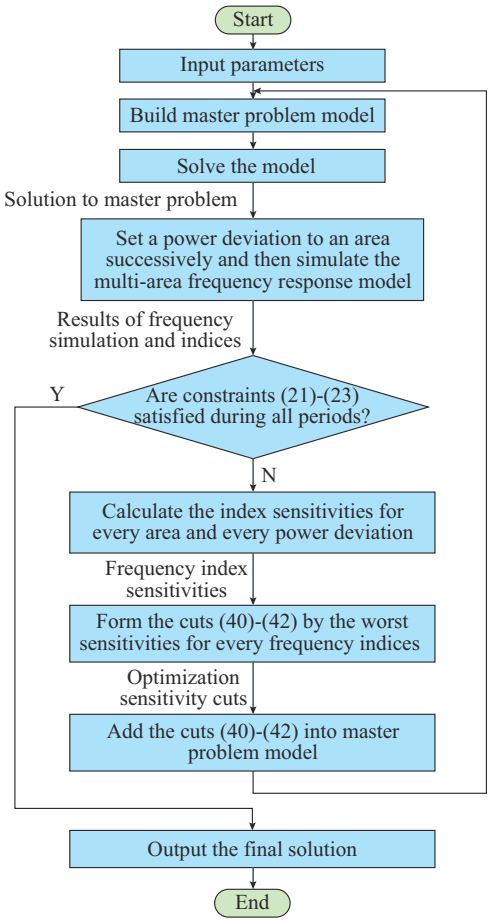

Fig. 3. Calculation flowchart of proposed sensitivity cuts for MFCUC.

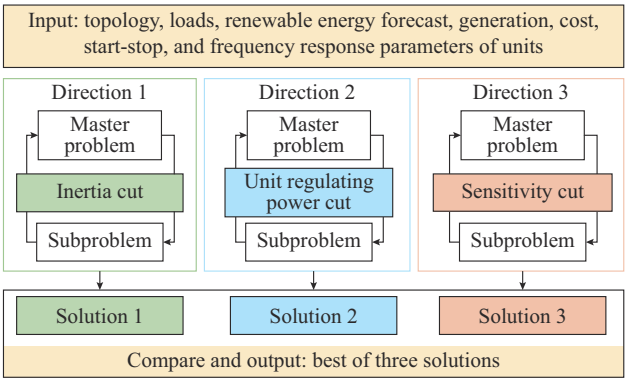

Fig. 4. Flowchart of proposed multi-direction method.

Generally, to apply the proposed MFCUC in the real world, the input parameters in Fig. 4 should be acquired firstly. Especially, the distribution of IM loads in the grid should be quantified precisely. Then, the frequency security

criterion should be set by the operators. Finally, the UC scheme can be solved as introduced in this section.

V. Case Study

To verify the effectiveness of the proposed model, case studies are performed on the modified three-area IEEE 39-bus system and the IEEE 118-bus system in this section. Figure 5 shows the topologies of the modified multi-area systems. All the system parameters can be found in [32]. In the modified systems, PV is installed on each load bus with the load proportion. Both wind power and PV power do not participate in frequency response. The forecast errors of load and RES are set to be ±5% and ±10%, respectively. The penalty factors C_{W} and C_{PV} are set to be 200 and 180 $\$\cdot\mathrm{MW}^{-1}\cdot\mathrm{h}^{-1}$, respectively.

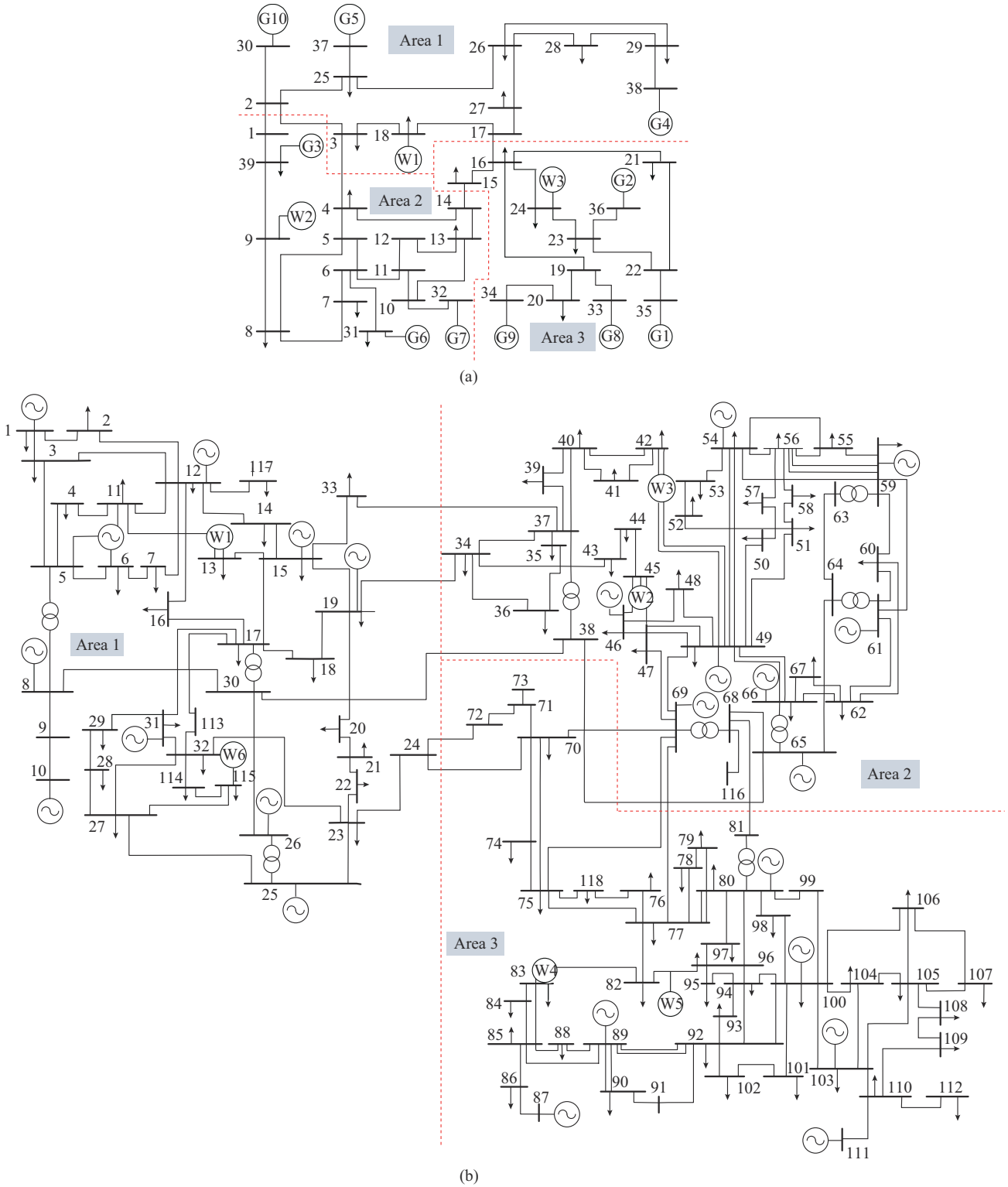

Fig. 5. Topologies of modified multi-area systems. (a) IEEE 39-bus system. (b) IEEE 118-bus system.

In this section, the master problem of MFCUC is solved by Gurobi, and the check of frequency constraints (21)-(23) in subproblems is performed with MATLAB/Simulink. In the Simulink settings, the step size is set to be 0.005 s, and the terminal time is 50 s. According to the simulation results, RoCoF is calculated as an average value in the first ten cycles, and f_∞ is the frequency at $t=50$ s. For the frequency security constraints in FCUC, $RoCoF_{\max}$, $f_{\text{nadir,min}}$, and $f_{\infty,\min}$ are set to be 0.50 Hz/s, 49.50 Hz, and 49.70 Hz, respectively. It should be noted that all the frequency indices in case studies are represented by the worst values among multiple areas at the same time.

The parameters of IMs in this paper are also listed in [32]. The rated power of IMs in area j is calculated as:

$$P_{N,j}^{\text{IM}}=\frac{\lambda\cdot\max\limits_{\tau}\left(\sum\limits_{k\in\Omega_j}P_{LN,k\tau}\right)}{Ke} \tag{46}$$

A. IEEE 39-bus System

To verify the effectiveness of FCUC with different optimization cuts, the following six cases are considered for comparison. The optimization cuts in Cases 2-4 are generated for the total frequency response resources in the power system, while the optimization cuts in Cases 5 and 6 are generated for each area. For example, in Case 2, a cut of the total inertia in the power system is generated for the master problem when the frequency security is not guaranteed. And in Case 5, the inertia cuts are generated for three areas, respectively.

Case 1: conventional UC without frequency constraints.

Case 2: MFCUC with the inertia cut for the total system.

Case 3: MFCUC with the unit regulating power cut for the total system.

Case 4: MFCUC with the proposed sensitivity cut.

Case 5: MFCUC with the inertia cuts for each area.

Case 6: MFCUC with the unit regulating power cut for each area.

Cases 2-6 are solved in the MAFR model with IMs. The simulation results of Cases 1-6 are compared in Table I. Figure 6 shows the three indices during each period among three areas for cases 1-4.

TABLE I
SIMULATION RESULTS OF CASES 1-6

Case	Iteration	$RoCoF_{\max}$ (Hz·s^{-1})	$f_{\text{nadir,min}}$ (Hz)	$f_{\infty,\min}$ (Hz)	Cost (M$)
Case 1		0.7683	49.3948	49.5868	1.2024
Case 2	8	0.4923	49.6068	49.7468	1.2159
Case 3	10	0.4923	49.6043	49.7416	1.2186
Case 4	4	0.4923	49.5932	49.7085	1.2146
Case 5			No solution		
Case 6					

From Table I, it is found that Case 1 provides the least operational cost. However, it can be found from Table I that Case 1 cannot avoid the violation of frequency security during the 8th-12th hours, while Cases 2-4 improve the frequency security with an incremental cost. The results of Fig. 6 verify that the frequency constraints can be satisfied with the proposed sensitivity cuts or with the cuts for increasing inertia and unit regulating power. Moreover, compared with Cases 2 and 3, Case 4 provides a more economical scheme for frequency security enhancement as the number of committed units with the on status is the lowest, as shown in Fig. 7.

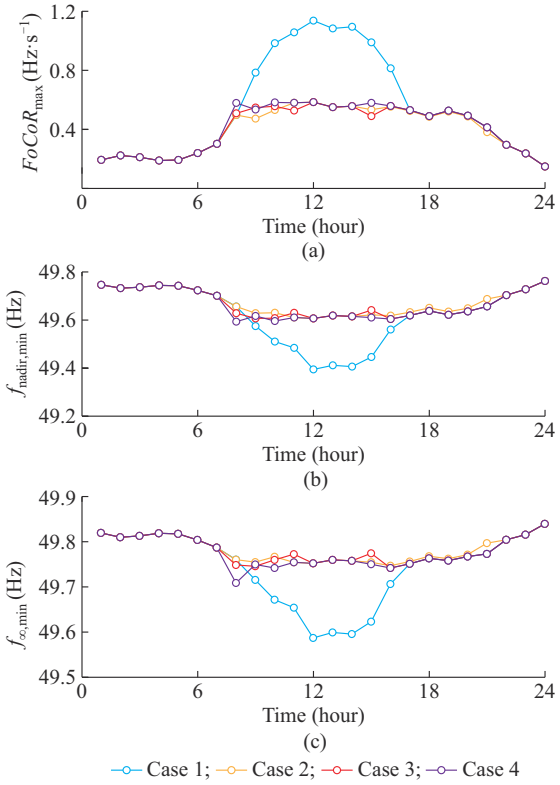

Fig. 6. Three indices during each period among three areas for Cases 1-4. (a) $RoCoF_{\max}$. (b) $f_{\text{nadir,min}}$. (c) $f_{\infty,\min}$.

The results also show that the optimization cuts in Cases 5 and 6 for each area may make the FCUC infeasible after several iterations. For example, after the first iteration of FCUC in Case 5, we have the frequency index $RoCoF_{2,11}$ as 0.5076 Hz/s and $RoCoF_{3,11}$ as 0.5056 Hz/s. This indicates that the limit of $RoCoF_{\max}$ is violated in areas 2 and 3 at the 11th hour. However, all the SG units in areas 2 and 3 have already started up at this time, which means it is impossible to further increase the inertia in areas 2 and 3. Thus, the result in Case 5 indicates no solution, which is similar to the iterations in Case 6. This indicates that it may not be practical in the MFCUC to generate the inertia cuts or the unit regulating power cuts for each area instead of the whole power system.

To illustrate the differences between the COI-based SFR model and the MAFR model in MFCUC, we consider the following Cases 7 and 8 for comparison with Case 4.

Case 7: FCUC with the proposed sensitivity cuts that consider the COI-based SFR model with IMs.

Case 8: frequency responses in the solution of Case 7 are simulated by the MAFR model.

Table II compares the simulation results of Cases 4, 7, and 8. Figure 8 shows the three indices during each period

among three areas. It can be observed from Table II and Fig. 8 that the FCUC with the COI-based SFR model is more economical than the MFCUC in Case 4, but it fails to guarantee the frequency security in each area. This illustrates that the COI-based SFR model may underestimate the risk of frequency violations in large power systems.

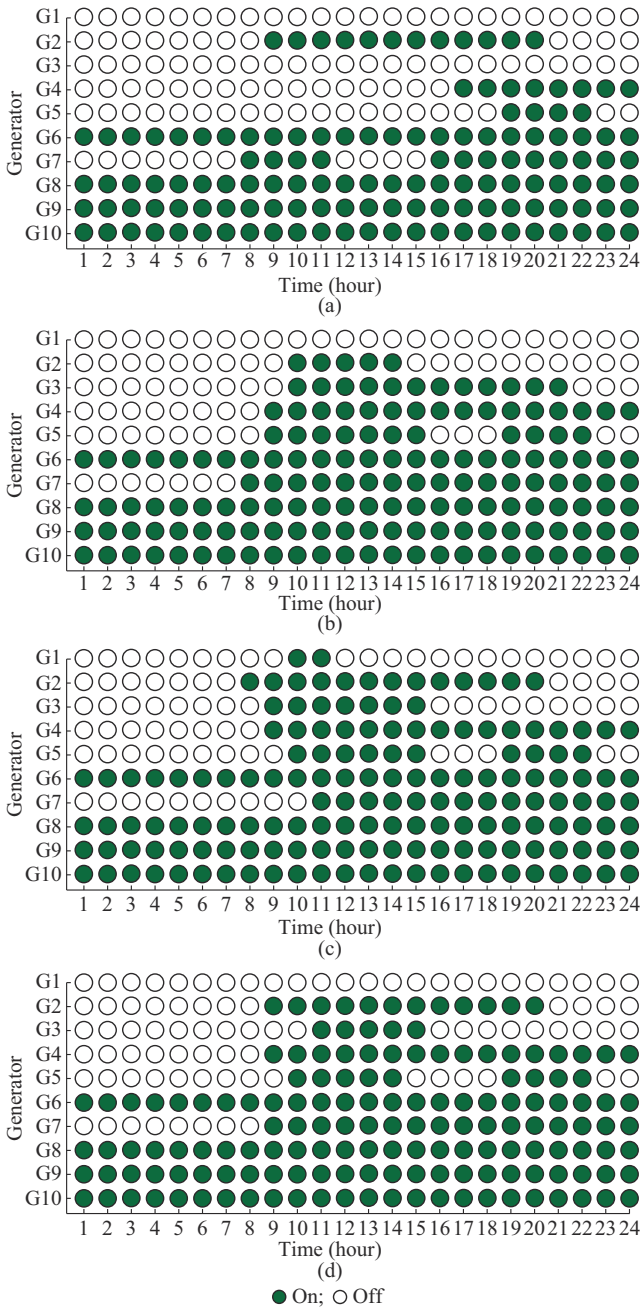

Fig. 7. UC schemes of Cases 1-4. (a) Case 1. (b) Case 2. (c) Case 3. (d) Case 4.

TABLE II
SIMULATION RESULTS OF CASES 4, 7, AND 8

Case	$RoCoF_{max}$ (Hz·s^{-1})	$f_{nadir,min}$ (Hz)	$f_{\infty,min}$ (Hz)	Cost (M$)
Case 4	0.4923	49.5932	49.7085	1.2146
Case 7	0.4209	49.5602	49.7031	1.2102
Case 8	0.5924	49.5698	49.7152	

To further illustrate the difference between the frequency response models in FCUC, we take the 9th hour in Fig. 8 as an example. When a power deviation occurs in area 1 at the 9th hour, the comparison of dynamic frequency responses between MAFR and COI-based SFR model is shown in Fig. 9.

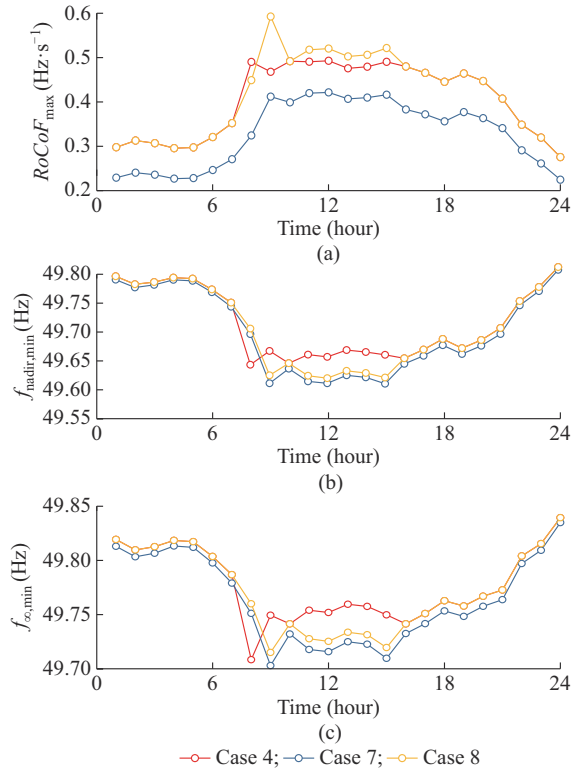

Fig. 8. Three indices during each period among three areas for Cases 4, 7, and 8. (a) $RoCoF_{max}$. (b) $f_{nadir,min}$. (c) $f_{\infty,min}$.

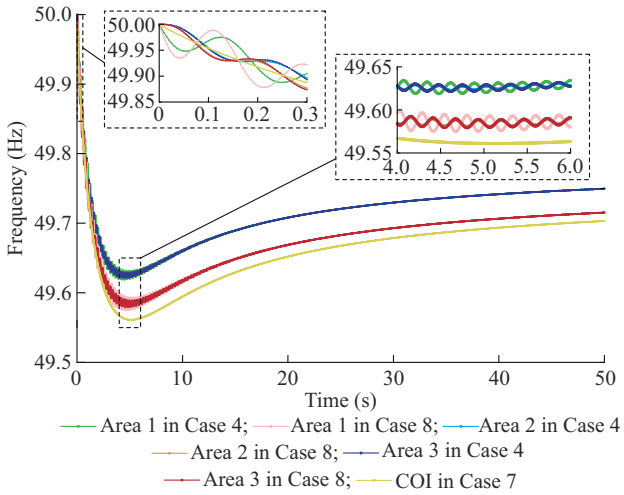

Fig. 9. Comparison of dynamic frequency response between MAFR and COI-based SFR model.

It is shown in Fig. 9 that the frequency starts to decrease after power deviation both in Cases 7 and 8. However, the COI-based SFR model only reflects the average dynamic frequency, while the MAFR model can capture the frequency differences between areas. As the power deviation occurs in area 1, it is the first area in which the frequency decreases

acutely. It is also noted that the frequency nadirs in the COI-based SFR model and the MAFR model are rather different. This is because a large amount of power is transmitted to area 1 from other areas when a power deviation occurs in area 1 in the MAFR model. However, these interactions are not modeled in the COI-based SFR model.

To illustrate the impact of IMs on frequency response, we consider the following cases for comparison. For simplicity, we set all the SG units committed at the 1st-24th hours in Cases 9 and 10.

Case 9: MAFR model with IMs.

Case 10: MAFR model without IMs.

Figure 10 shows three indices during each period among three areas for Cases 9 and 10. It can be found from Fig. 10 that the $RoCoF_{max}$ and $f_{nadir,min}$ are improved in Case 9 compared with those in Case 10. In addition, $f_{\infty,min}$ in Case 9 is almost the same as that in Case 10. This indicates that the inertia of IMs mainly enhances the early stage of the frequency response of power systems. This can be significant for power systems with high penetration of RESs, since most cascading trips of RESs are induced by violations of RoCoF or f_{nadir} limits.

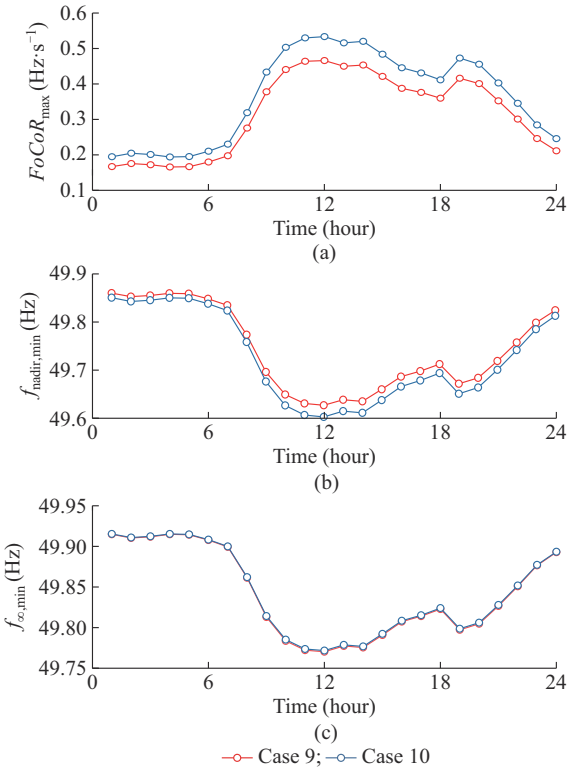

Fig. 10. Three indices during each period among three areas for Cases 9 and 10. (a) $RoCoF_{max}$. (b) $f_{nadir,min}$. (c) $f_{\infty,min}$.

We also take the 12nd hour as an example to compare the dynamic frequency response in Cases 9 and 10. The simulation is performed with a power deviation in area 3, and the results are shown in Fig. 11. It can be clearly observed that the IMs can provide inertia to improve the frequency response but do not participate in the PFR.

Finally, Case 11 is considered to further illustrate the impact of IMs on MFCUC.

Case 11: MFCUC with the proposed sensitivity cut, in which λ is set to be 0.3 and the other parameters are the same as those in Case 4.

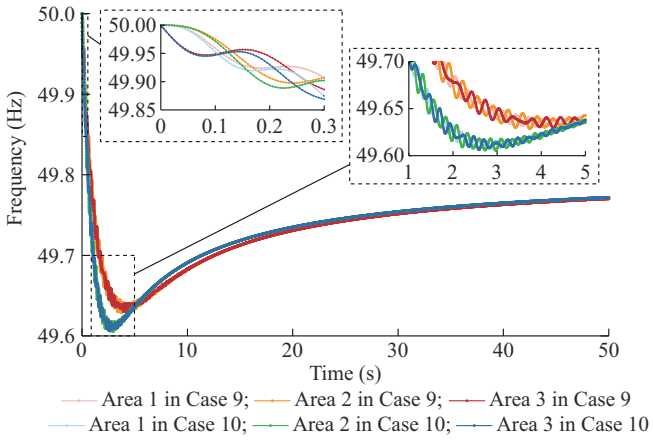

Fig. 11. Comparison of dynamic frequency response between Cases 9 and 10.

Table III compares the simulation results of Cases 4 and 11. Figure 12 compares the inertia provided by SGs for each area during each period. The results indicate that the demand for inertia from SGs decreases with the increment of λ. Thus, the consideration of the inertia of IMs can help reduce the operational cost in FCUC.

TABLE III
SIMULATION RESULTS OF CASES 4 AND 11

Cases	λ	$RoCoF_{max}$ (Hz·s^{-1})	$f_{nadir,min}$ (Hz)	$f_{\infty,min}$ (Hz)	Cost (M$)
Case 4	0.6	0.4923	49.5932	49.7085	1.2146
Case 11	0.3	0.4981	49.6048	49.7497	1.2213

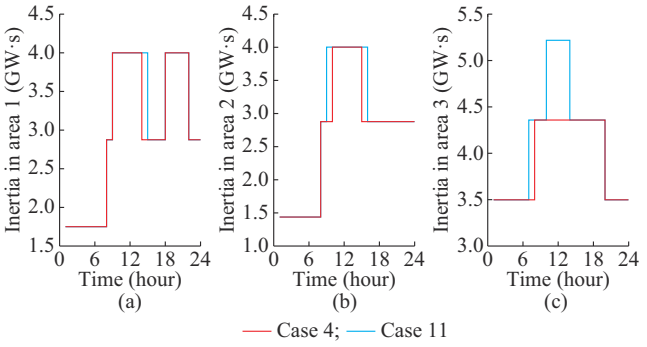

Fig. 12. Inertia provided by SGs for each area during each period. (a) Area 1. (b) Area 2. (c) Area 3.

B. IEEE 118-bus System

In this subsection, we further validate the proposed MFCUC model on the IEEE 118-bus system. Similar to Section V-A, the following Cases 12-16 are considered.

Case 12: conventional UC without frequency constraints for the IEEE 118-bus system.

Case 13: MFCUC with the inertia cut for the total system, in which the inertia of IMs is considered in the MAFR mod-

el.

Case 14: MFCUC with the unit regulating power cut for the total system, in which the inertia of IMs is considered in the MAFR model.

Case 15: MFCUC with the proposed sensitivity cut, in which the inertia of IMs is considered in the MAFR model.

Case 16: MFCUC with the proposed sensitivity cut, in which the inertia of IMs is not considered in the MAFR model.

Table IV shows the simulation results of Cases 12-16. And Fig. 13 shows three indices during each period among three areas for Cases 12-16.

TABLE IV
SIMULATION RESULTS OF CASES 12-16

Cases	Iteration	$RoCoF_{max}$ (Hz·s^{-1})	$f_{nadir,min}$ (Hz)	$f_{\infty,min}$ (Hz)	Cost (M$)
Case 12		0.8310	49.3082	49.6195	6.9891
Case 13	50	0.4981	49.5763	49.8054	7.4782
Case 14	44	0.4982	49.5744	49.8022	7.4864
Case 15	40	0.4997	49.5016	49.7392	7.0795
Case 16	5	0.4181	49.5310	49.7512	7.2294

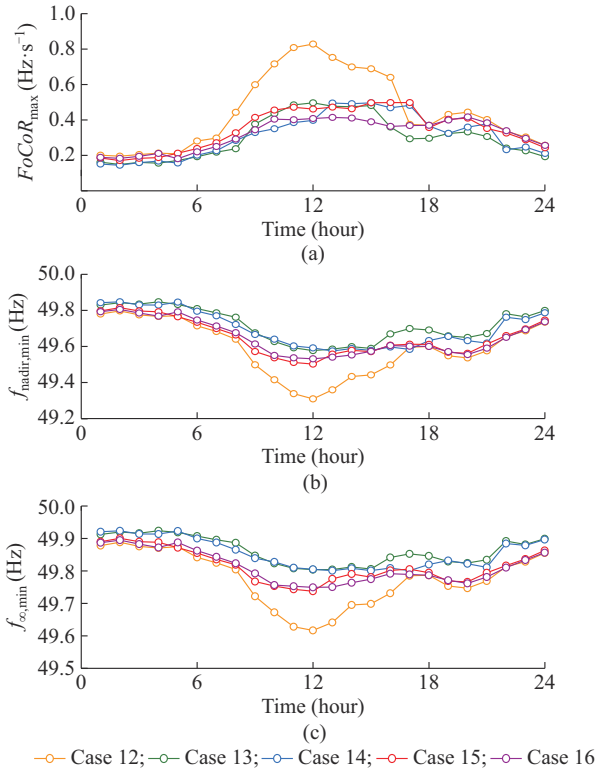

Fig. 13. Three indices during each period among three areas for Cases 12-16. (a) $RoCoF_{max}$. (b) $f_{nadir,min}$. (c) $f_{\infty,min}$.

It can be observed from Table IV and Fig. 13 that the system frequency indices in Case 12 are significantly lower than their thresholds as they do not consider the frequency constraints. On the contrary, the frequency constraints are not violated in Cases 13-16 with the varying degrees of cost increments.

The results also show that the cost increments in Cases 15 and 16 are slighter than those in Cases 13 and 14. The slightest cost increment is 1.3% in Case 15 while the greatest one is 7.1% in Case 14. The reason is that the proposed sensitivity cut can help the operators improve the uniformity of the inertia distribution in the multi-area power system while the operators are required to increase the total inertia due to inertia cut or the unit regulating power cut. As a result, the increment of the number of committed units is less when the sensitivity cut is considered. Additionally, the UC in Case 15 is more economical than that in Case 16 as the inertia of IMs is considered.

VI. CONCLUSION

In this paper, an MFCUC considering the MAFR model with the inertia of IMs is developed to address the frequency security issues of power systems with a high penetration of RESs. To solve the proposed MFCUC, this paper proposes a multi-direction optimization framework with sensitivity cuts. The conclusions are drawn as follows.

1) The proposed MFCUC is more precise than traditional FCUC with the COI-based SFR model. It can capture the spatial distribution characteristic of frequency response and thus avoid underestimating frequency violation risk.

2) The consideration of IMs in the MFCUC can enhance the frequency response with the improvement of the RoCoF index and frequency nadir index, which may reduce the operational cost of power systems compared with the MFCUC without the consideration of IMs.

3) The proposed sensitivity cuts can further improve the robustness of the decomposition algorithm for solving the nonlinear MFCUC, especially when it is not practical to generate the traditional cuts of inertia and unit regulating capacity for each area instead of the whole power system in MFCUC.

REFERENCES

[1] Z. Zhou, L. Shi, and Y. Chen, "An optimal over-frequency generator tripping strategy for regional power grid with high penetration level of renewable energy," *Journal of Modern Power Systems and Clean Energy*, vol. 9, no. 5, pp. 1007-1017, Sept. 2021.

[2] R. Yan, T. K. Saha, F. Bai *et al.*, "The anatomy of the 2016 south Australia blackout: a catastrophic event in a high renewable network," *IEEE Transactions on Power Systems*, vol. 33, no. 5, pp. 5374-5388, Sept. 2018.

[3] NGESO. (2019, Sept.). Technical report on the events of 9 August 2019. [Online]. Available: https://www.ofgem.gov.uk/system/files/docs/2019/09/esotechnicalreport-final.pdf

[4] F. Milano and Á. O. Manjavacas, "Frequency-dependent model for transient stability analysis," *IEEE Transactions on Power Systems*, vol. 34, no. 1, pp. 806-809, Jan. 2019.

[5] M. L. Chan, R. D. Dunlop, and F. Schweppe, "Dynamic equivalents for average system frequency behavior following major distribances," *IEEE Transactions on Power Apparatus and Systems*, vol. PAS-91, no. 4, pp. 1637-1642, Jul. 1972.

[6] P. M. Anderson and M. Mirheydar, "A low-order system frequency response model," *IEEE Transactions on Power Systems*, vol. 5, no. 3, pp. 720-729. Aug. 1990.

[7] L. Badesa, F. Teng, and G. Strbac, "Conditions for regional frequency stability in power system scheduling – Part I: theory," *IEEE Transactions on Power Systems*, vol. 36, no. 6, pp. 5558-5566, Nov. 2021.

[8] L. Che, X. Shen, and M. Shahidelpour, "Primary frequency response based rescheduling for enhancing microgrid resilience," *Journal of Modern Power Systems and Clean Energy*, vol. 7, no. 4, pp. 696-704, Jul. 2019.

[9] H. Gu, R. Yan, T. K. Saha *et al*., "System strength and inertia constrained optimal generator dispatch under high renewable penetration," *IEEE Transactions on Sustainable Energy*, vol. 11, no. 4, pp. 2392-2406, Oct. 2020.
[10] C. Mosca, E. Bompard, G. Chicco *et al*., "Technical and economic impact of the inertia constraints on power plant unit commitment," *IEEE Open Access Journal of Power and Energy*, vol. 7, pp. 441-452, Oct. 2020.
[11] J. Lu, Y. Mao, L. Liu *et al*., "Unit commitment of power system with wind power and photovoltaic considering frequency safety constraint," in *Proceedings of 2021 IEEE Sustainable Power and Energy Conference (iSPEC)*, Nanjing, China, Dec. 2021, pp. 1486-1493.
[12] Y. Zhang, H. Cui, J. Liu *et al*., "Encoding frequency constraints in preventive unit commitment using deep learning with region-of-interest active sampling," *IEEE Transactions on Power Systems*, vol. 37, no. 3, pp. 1942-1955, May 2022.
[13] D. T. Lagos and N. D. Hatziargyriou, "Data-driven frequency dynamic unit commitment for island systems with high RES penetration," *IEEE Transactions on Power Systems*, vol. 36, no. 5, pp. 4699-4711, Sept. 2021.
[14] N. Nguyen, V. Johnson, and J. Mitra, "Environmental-economic dispatch of power system in the presence of wind generation," in *Proceedings of 2015 North American Power Symposium (NAPS)*, Charlotte, USA, Oct. 2015, pp. 1-6.
[15] C. J. Ferrandon-Cervantes, B. Kazemtabrizi, and M. C. M. Troffaes, "Inclusion of frequency stability constraints in unit commitment using separable programming," *Electric Power Systems Research*, vol. 203, p. 107669, Feb. 2022.
[16] C. Zhang, L. Liu, H. Cheng *et al*., "Frequency-constrained co-planning of generation and energy storage with high-penetration renewable energy," *Journal of Modern Power Systems and Clean Energy*, vol. 9, no. 4, pp. 760-775, Jun. 2021.
[17] H. Ahmadi and H. Ghasemi, "Security-constrained unit commitment with linearized system frequency limit constraints," *IEEE Transactions on Power Systems*, vol. 29, no. 4, pp. 1536-1545, Jul. 2014.
[18] S. S. Oskouee, S. Kamali, and T. Amraee, "Primary frequency support in unit commitment using a multi-area frequency model with flywheel energy storage," *IEEE Transactions on Power Systems*, vol. 36, no. 6, pp. 5105-5119, Apr. 2021.
[19] F. Perez-Illanes, E. Alvarez-Miranda, C. Rahmann *et al*., "Robust unit commitment including frequency stability constraints," *Energies*, vol. 9, no. 11, pp. Nov. 2016.
[20] N. Yang, Z. Dong, L. Wu *et al*., "A comprehensive review of security-constrained unit commitment," *Journal of Modern Power Systems and Clean Energy*, vol. 10, no. 3, pp. 562-576, May 2022.
[21] Y. Yang, J. Peng, C. Ye *et al*., "A criterion and stochastic unit commitment towards frequency resilience of power systems," *IEEE Transactions on Power Systems*, vol. 37, no. 1, pp. 640-652, Jul. 2021.
[22] S. Jiang, X. Zhao, G. Pan *et al*., "A novel robust frequency-constrained unit commitment model with emergency control of HVDC," *Energy Reports*, vol. 8, pp. 57-67, Oct. 2022.
[23] J. Ye, T. Lin, R. Bi *et al*., "Unit commitment in isolated grid considering dynamic frequency constraint," in *Proceedings of 2016 IEEE PES General Meeting (PESGM)*, Boston, USA, Jul. 2016, pp. 1-5.
[24] D. Wang and X. Yuan, "Available inertia estimation of induction machine in electromechanical timescale and its effects on frequency dynamics of power systems with renewable energy," *Proceedings of CSEE*, vol. 38, no. 24, pp. 7258-7266, Dec. 2018.
[25] D. Wang, X. Yuan, W. Shen *et al*., "Available inertia estimation of induction machine and its effect on frequency response of power systems with wind penetration," in *Proceedings of 2019 IEEE Innovative Smart Grid Technologies – Asia (ISGT Asia)*, Chengdu, China, May 2019, pp. 1783-1787.
[26] Y. Wen, J. Zhan, C. Y. Chung *et al*., "Frequency stability enhancement of integrated AC/VSC-MTDC systems with massive infeed of offshore wind generation," *IEEE Transactions on Power Systems*, vol. 33, no. 5, pp. 5135-5146, Sept. 2018.
[27] O. I. Elgerd. and C. E. Fosha, "Optimum megawatt-frequency control of multiarea electric energy systems," *IEEE Transactions on Power Apparatus and Systems*, vol. PAS-89, no. 4, pp. 556-563, Apr. 1970.
[28] Q. Yang, J. Wang, H. Yin *et al*., "A fast calculation method for long-term security-constrained unit commitment of large-scale power systems with renewable energy," *Journal of Modern Power Systems and Clean Energy*, vol. 10, no. 5, pp. 1127-1137, Sept. 2022.
[29] M. Ban, J. Yu, M. Shahidehpour *et al*., "Integration of power-to-hydrogen in day-ahead security-constrained unit commitment with high wind penetration," *Journal of Modern Power Systems and Clean Energy*, vol. 5, no. 3, pp. 337-349, May 2017.
[30] R. Lu, T. Ding, B. Qin *et al*., "Multi-stage stochastic programming to joint economic dispatch for energy and reserve with uncertain renewable energy," *IEEE Transactions on Sustainable Energy*, vol. 11, no. 3, pp. 1140-1151, Jul. 2020.
[31] T. Amraee, M. G. Darebaghi, A. Soroudi *et al*., "Probabilistic under frequency load shedding considering RoCoF relays of distributed generators," *IEEE Transactions on Power Systems*, vol. 33, no. 4, pp. 3587-3598, Jul. 2018.
[32] LX2000Xu. (2023, Jan.). Input parameters. [online]. Available: https://github.com/LX2000Xu/Data

Leibao Wang received the B.E. degree in electrical engineering from Xi'an Jiaotong University, Xi'an, China, in 2016, and the Ph.D. degree in electrical engineering from Chongqing University, Chongqing, China, in 2021. In 2020, he was a Visiting Scholar with the Stevens Institute of Technology, Hoboken, USA. He is currently an Engineer with the State Grid Hebei Electric Power Research Institute, Shijiazhuang, China. His main research interests include power system reliability and cascading failures.

Hui Fan received the B.S. degree in electrical engineering from North China Electric Power University, Baoding, China, in 1991, and the M.S. degree in electric power system and automation from North China Electric Power University, Beijing, China, in 1998. From 1991 to 2018, he has successively served as an Engineer and a Senior Engineer at the State Grid Hebei Electric Power Research Institute, Shijiazhuang, China, where he was a Professor-level Senior Engineer from 2018 to 2020. Since 2020, he has been serving as the Director of the Hebei Province Energy Internet Simulation Modeling and Control Key Laboratory, North China Electric Power University, where he has served as a Postgraduate Tutor. His research interests include power system simulation modeling and control, microgrids, and power electronic control.

Jifeng Liang received the M.S. degree from North China Electric Power University, Beijing, China. He is currently a Senior Engineer with the State Grid Hebei Electric Power Research Institute, Shijiazhuang, China. His research interests include power system security analysis and new energy technology.

Longxun Xu received the B.S. degree from Chongqing University, Chongqing, China, in 2021. He is currently working toward the Ph.D. degree with the School of Electrical Engineering, Chongqing University. His current research interests include risk modeling and operation optimization in power system.

Tiecheng Li received the M.S. degree in electrical engineering from North China Electric Power University, Baoding, China, in 2007. From 2007 to 2020, he was an Engineer with State Grid Hebei Electrical Power Company Research Institute, Shijiazhuang, China. His research interest includes relay protection control.

Peng Luo received the Ph.D. degree from Tianjin University, Tianjin, China, in 2012. He is currently working with the State Grid Hebei Electric Power Research Institute, Shijiazhuang, China. His main research interests include power system automation, new energy power systems, and intelligent power distribution.

Bo Hu received the Ph.D. degree in electrical engineering from Chongqing University, Chongqing, China, in 2010, where he is currently a Full Professor with the School of Electrical Engineering. He is the Editor of the IEEE Transactions on Power Systems and IEEE Power Engineering Letters. His research interests include power system reliability and parallel computing in power systems.

Kaigui Xie received the Ph.D. degree in electrical engineering from Chongqing University, Chongqing, China, in 2001. He is currently working as a Full Professor with the School of Electrical Engineering. His main research interests include power system reliability, planning, and analysis.